O··H··O distance was increased to 3.50 Å, from 2.70 Å in (R), and ν(O····O stretch, at 248 cm^{-1}) was taken as the reaction coordinate. The other interatomic distances and vibrational frequencies were assumed to be mean values between those of [t] and [R], with E° = 14.1 kcal mol^{-1}; a collision cross-section of 6.86 Å was estimated; λ = 1, and the Whitten-Rabinovitch state count was used. The results for log k_{uni} vs. log P (torr) are plotted in Figure 3. Below 10 torr the system follows second-order kinetics. At T = 260 K and P = 2.5 torr, k_{uni} = 17 s^{-1}. Another set of curves calculated with E° = 12 kcal mol^{-1} gave k_{uni} [T = 260; P = 2.5 torr] = 380 s^{-1}. At 260 K, $K^{(p)}$ = 1.036 × 10^{-4} atm and $K^{(c)}$ = 4.856 × 10^{-9} mol cm^{-3};[9] and for a room temperature fill of 2.5 torr, $[t]_{eq}^{260}$ = 2.44 × 10^{-8} mol cm^{-3}. Hence $\tau_{chem}^{calcd}(E^\circ = 12)$ = 2.38 × 10^{-4} s and $\tau_{chem}^{calcd}(E^\circ = 14.1)$ = 5.32 × 10^{-3} s.

The absence of a characteristic coalescence feature in the many numerous scans we recorded indicates that for the ^1H_O exchange $\tau_{NMR} \leq 2 \times 10^{-4}$ s, since $\Delta\nu$ = 1170 Hz at 300 MHz for the monomer vs. dimer chemical shifts. This is not consistent with E° = 14.1 kcal mol^{-1}; rather it indicates that E° is somewhat less than 12 kcal mol^{-1}. However, one can argue that no serious discrepancy with the thermochemical value exists. Note that $E^\circ = \Delta H^\circ_0 = \Delta H^\circ_{300} - \int_0^{300} \Delta C_p \, dT$. The heat capacity correction term is about 1.5 kcal, which may be added to the negative extreme of the quoted error limit (-1.5 kcal).

Our conclusions are the following: (a) There is no detectable barrier to dissociation of the dimer. In that respect the present data are more definitive than the conclusion reached for the $(CH_3)_2O$·HCl dissociation.[21] (b) It is likely that a factor of 5-10 increase in NMR sensitivity would permit determination of the dimer/monomer dissociation relaxation time. (c) At pressures below 10 torr, RRKM calculations indicate that the dissociation follows second-order kinetics; i.e., upon association of two [t] monomers the dimer must get de-excited by collision with the third body within less than a nanosecond.

Acknowledgment. These studies were funded by the AFOSR under Grant No. AFOSR-80-0046. We acknowledge the National Science Foundation Instrumentation Program (CHE-79-04825 and PCM-80-18643) for support of the Cornell Nuclear Magnetic Resonance Facility.

Registry No. HCOOH, 64-18-6.

(21) Bauer, S. H.; et al. *J. Am. Chem. Soc.* **1985**, *107*, 743.

Resonance Raman Studies of the Excited Electronic States of $(CN)_5Fe^{III}$(imidazole)$^{2-}$ and $(NH_3)_5Ru^{III}$(imidazole)$^{3+}$

Colleen M. Jones, Craig R. Johnson, Sanford A. Asher,* and Rex E. Shepherd

Contribution from the University of Pittsburgh, Department of Chemistry, Pittsburgh, Pennsylvania 15260. *Received December 17, 1984*

Abstract: UV and visible wavelength resonance Raman spectra and Raman excitation profiles were used to assign the electronic transitions of the imidazole (imH) complexes of $(CN)_5Fe^{2+}$ and $(NH_3)_5Ru^{3+}$. This study demonstrates, for the first time, the ability of resonance Raman excitation profiles to distinguish between the π orbitals involved in imidazole-metal charge-transfer transitions (LMCT). LMCT transitions observed in the absorption spectrum at 475 (Fe) and 425 nm (Ru) involve the imidazole π_1 orbital which has major electron density associated with the carbon atoms of the ring. The 403 (Fe) and 297 nm (Ru) LMCT transitions involve transitions from the π_2 imidazole orbital which has high electron density associated with the nitrogen atoms. The imidazole ring modes of the $(CN)_5Fe(imH)^{2-}$ and $(NH_3)_5Ru(imH)^{3+}$ complexes are selectively enhanced by these LMCT transitions. The Fe complex has an additional absorption band at 356 nm that is not present in the Ru complex. Excitation within this band results in the exclusive enhancement of the C≡N stretch and a broad low-frequency Fe—(C≡N) vibration; thus, the 356-nm absorption band is assigned to a $d\pi_{(Fe)} \leftarrow$ CN LMCT. The C≡N stretch is also enhanced within the 403 and 475 nm absorption bands which indicate a strong mixing of the iron and cyanide π orbitals. From the frequency sensitivity to imH deuteration and methyl substitution we tentatively assign the 265-cm^{-1} vibration of $(CN)_5Fe(imH)^{2-}$ to a Fe-N(imH) stretching vibration. It is unlikely that excitation into similar LMCT transitions in heme proteins such as hemoglobin will result in sufficient Raman intensity to permit studies of proximal histidine-heme interactions.

The unique ability of resonance Raman spectroscopy to study the coordination environment of transition metals in proteins derives from its high selectivity and sensitivity.[1] Raman excitation within charge-transfer transitions gives a selective enhancement of internal ligand and metal-ligand stretching vibrations. These data provide important information concerning protein active sites. In addition to its utility as a structural probe of metal sites in proteins, resonance Raman spectroscopy, particularly resonance Raman excitation profiles, provides a powerful technique to aid in the assignment of electronic transitions. Resonant excitation within an absorption band results in the enhancement of only those modes which are coupled to the electronic transition.[2]

Imidazole complexes of transition metals are of particular biological interest because the imidazole side chain of the amino acid histidine often binds to metal centers in proteins. The interest in iron-imidazole bonding and interactions derives in part from the ubiquitous presence of imidazole-iron porphyrin complexes in heme proteins and the possible involvement of this linkage in the cooperativity mechanism of hemoglobin.[3]

This work characterizes the resonance Raman excitation profile of the LMCT transitions[4] of $(CN)_5Fe^{III}imH^{2-}$ and $(NH_3)_5Ru^{III}imH^{3+}$ and provides a basis for similar studies on heme

(1) Parker, F. S. "Applications of Infrared, Raman, and Resonance Raman Spectroscopy in Biochemistry"; Plenum Press: New York, 1983. Tu, A. T. "Raman Spectroscopy in Biology: Principles and Applications"; John Wiley and Sons: New York, 1982. Carey, P. R. "Biochemical Applications of Raman and Resonance Raman Spectroscopies"; Academic Press: New York, 1982. Asher, S. A. *Methods Enzymology* **1981**, *76*, 371-413. Kitagawa, T.; Ozaki, Y.; Kyogoku, Y. *Adv. Biophys.* **1978**, *11*, 153-196.

(2) Asher, S. A.; Sauer, K. *J. Chem. Phys.* **1976**, *64*, 4115-4125.

(3) Perutz, M. F. *Nature (London)* **1972**, *237*, 495-499. Nagai, K.; Kitagawa, T. *Proc. Natl. Acad. Sci. U.S.A.* **1980**, *77*, 2033-2037.

(4) Johnson, C. R.; Henderson, W. W.; Shepherd, R. E. *Inorg. Chem.* **1984**, *23*, 2754-2763.

0002-7863/85/1507-3772$01.50/0

proteins. $(CN)_5Fe(imH)^{2-}$ structurally mimics the ligand binding site of hemoglobin. It is geometrically and electronically similar to the heme center of hemoglobin. The four planar cyanides of the iron complex approximate the σ donating and π backbonding abilities of the porphyrin ring. The visible electronic spectrum of $(CN)_5Fe(imH)^{2-}$ is not complicated by the $\pi^* \leftarrow \pi$ transitions which dominate the spectra of heme complexes, and possibly mask charge-transfer transitions involving the histidine ligand. In addition, low-spin d^5 complexes such as $(CN)_5Fe(imH)^{2-}$ and $(NH_3)_5Ru(imH)^{3+}$ are ideally suited for studying charge-transfer transitions.[5] The lowest energy charge-transfer transitions in these complexes are from a filled molecular orbital of imH to the single vacancy in the $d\pi_{(Fe)}$ orbitals of the metal. Since there is one unpaired electron in both the ground and excited states, the relative energies of the ligand HOMO's may be inferred directly from the energies of the electronic transitions.[5]

There has been some success in identifying charge-transfer transitions in the spectra of metmyoglobin and methemoglobin derivatives such as the azide, fluoride, and hydroxide complexes.[6] Recently, Nagai et al.[7] have demonstrated the enhancement of the ligated tyrosinate in hemoglobins M Boston and M Iwate. Enhancement of the tyrosinate ring vibrations results from a tyrosine → heme LMCT transition. Ondrias et al. have recently proposed that an Fe–histidine charge-transfer band lies buried to the blue side of the Soret band of heme proteins.[8] In contrast, Bangcharoenpaurpong et al. suggest that the enhancement of the Fe-proximal histidine vibration derives from the heme $\pi^* \leftarrow \pi$ Soret transition.[9] Wright et al. have identified an iron-to-pyridine charge-transfer transition in a bispyridine iron(II) heme by resonance Raman spectroscopy.[10] They observed enhancement of pyridine modes and of an Fe–pyridine stretching mode with excitation within a band at ~490 nm assigned to a $\pi^*_{(py)} \leftarrow d\pi_{(Fe)}$ charge-transfer transition. A similar charge-transfer transition for an imidazole–iron(II) heme would be expected to occur in the UV since imidazole is a considerably poorer π acceptor than pyridine.[11] Imidazole complexes of iron(III) hemes would be expected to exhibit LMCT transitions similar to those of $(CN)_5Fe(imH)^{2-}$. The iron–imidazole stretch of oxymyoglobin and oxyhemoglobin has not been identified, and imidazole to iron charge-transfer transitions have not been located for these proteins. If proximal histidine to heme iron LMCT transitions could be utilized to enhance the vibrational spectrum of the histidine, subtle alterations in histidine hydrogen bonding to the protein, as well as geometric alterations of the heme, could be probed to help elucidate protein structure and the enzymatic mechanism.

We find that imidazole vibrations are enhanced with excitation within the LMCT transitions involving imidazole π orbitals of $(CN)_5Fe(imH)^{2-}$ and $(NH_3)_5Ru(imH)^{3+}$; however, these enhancements are only moderate. Walters and Spiro recently reported a resonance Raman study of $(CN)_5Fe(imH)^{2-}$.[12] Many of our conclusions parallel those of Walters and Spiro; however, our more detailed excitation profiles of $(CN)_5Fe(imH)^{2-}$ and the new $(NH_3)_5Ru(imH)^{3+}$ excitation profile data lead us to different assignments for the electronic transition.

Experimental Section

Sample solutions of imidazole complexes of $[(CN)_5Fe^{III}]^{2-}$ were prepared either by dissolving calcium salts of these complexes in water or by direct synthesis of the complexes in solution. $[Na_3(CN)_5Fe^{II}NH_3]\cdot 3H_2O$, the starting material for the preparation of the imidazole complexes, was prepared by using the procedures followed by Shepherd.[13] Imidazole and various methylated imidazoles were obtained from Aldrich. The $(CN)_5Fe^{III}imH^{2-}$ complex was prepared by oxidation of the Fe(II) complex with H_2O_2.[13c] Calcium salts were formed by crystallizing the complex from a saturated $CaCl_2$ solution.[14] Excitation profile data were obtained from solutions prepared from the calcium salts.

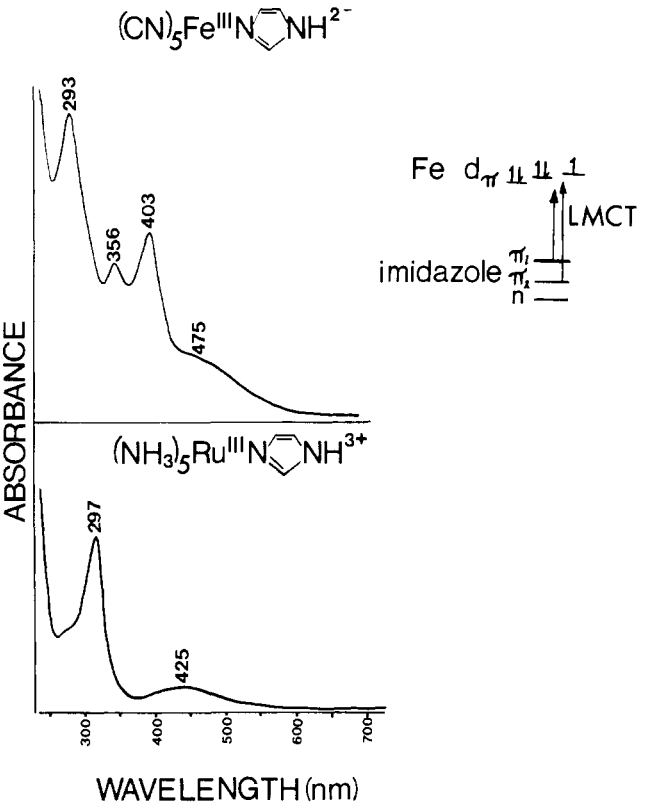

Figure 1. UV-visible absorption spectra of aqueous solutions of $(CN)_5Fe(imH)^{2-}$ and $(NH_3)_5Ru(imH)^{3+}$. An energy-level diagram indicates the ligand-to-metal charge-transfer transitions (LMCT) from the imidazole π orbitals to the iron π-type orbitals. The spectra are not displayed on the same absorption scale.

The introduction of Na_2SO_4 as an internal standard to the aqueous samples resulted in the formation of a $CaSO_4$ precipitate which was filtered off prior to the Raman spectral measurements. The $[(NH_3)_5Ru^{III}]^{3+}$ imidazole complexes (chloride salts) were prepared by using published procedures.[15] Samples were checked for photodecomposition by comparing the absorption spectra before and after laser irradiation. No evidence of photodecomposition was observed. $[(Bu)_4N]_3[(CN)_5Fe^{III}SCN]$ and $[(Bu)_4N]_3[(CN)_5Fe^{III}(N_3)]$ were prepared by following the procedures of Gutterman and Gray.[16]

Deuterated imidazole was prepared in a manner similar to that of Kincaid et al.[17] Imidazole was purified by vacuum sublimation and dissolved in slightly acidic D_2O (Aldrich). The solution was sealed and heated to 150 °C for approximately 24 h, the D_2O was evaporated off, and the deuterated imidazole was collected by vacuum sublimation. NMR and mass spectral data showed that the imidazole was at least 80% deuterated.

The deuterated imidazole complex of $[(CN)_5Fe^{III}]^{2-}$ was prepared by adding a 10% excess of the deuterated imidazole to a solution of $Na_3(CN)_5Fe^{II}NH_3$ in D_2O. A 10% excess of KIO_4 (Aldrich) was added to oxidize the complex, and the pD of the solution was adjusted to 7 ± 1 pD units with DCl. Addition of KI (Mallinckrodt) was necessary to

(5) Rowe, M. D.; McCaffery, A. J.; Gale, R.; Copsey, D. N. *Inorg. Chem.* **1972**, *11*, 3090–3098.
(6) Asher, S. A.; Vickery, L. E.; Schuster, T. M.; Sauer, K. *Biochemistry* **1977**, *16*, 5849–5856. Asher, S. A.; Schuster, T. M. *Biochemistry* **1979**, *18*, 5377–5387.
(7) Nagai, K.; Kagimoto, T.; Hayashi, A.; Taketa, F.; Kitagawa, T. *Biochemistry* **1983**, *22*, 1305–1311.
(8) Ondrias, M. R.; Rousseau, D. L.; Simon, S. R. *J. Biol. Chem.* **1983**, *258*, 5638–5642.
(9) Bangcharoenpaurpong, O.; Schomacker, K. T.; Champion, P. M. *J. Am. Chem. Soc.* **1984**, *106*, 5688–5698.
(10) Wright, P. G.; Stein, P.; Burke, J. M.; Spiro, T. G. *J. Am. Chem. Soc.* **1979**, *101*, 3531–3535.
(11) Johnson, C. R.; Shepherd, R. E. *Inorg. Chem.* **1983**, *22*, 3506–3513.
(12) Walters, M. A.; Spiro, T. G. *Inorg. Chem.* **1983**, *22*, 4014–4017.
(13) (a) Shepherd, R. E. *J. Am. Chem. Soc.* **1976**, *98*, 3329–3335. (b) Brauer, G. "Handbook of Preparative Inorganic Chemistry", 2nd ed.; Academic Press: New York, 1965; vol. 2, p 1511. (c) Johnson, C. R.; Shepherd, R. E.; Marr, B.; O'Donnell, S.; Dressick, W. *J. Am. Chem. Soc.* **1980**, *102*, 6227–6235.
(14) Johnson, C. R.; Shepherd, R. E. *Synth. React. Inorg. Met.-Org. Chem.* **1984**, *14*, 339–353.
(15) Sundberg, R. J.; Bryan, R. F.; Taylor, I. F.; Taube, H. *J. Am. Chem. Soc.* **1974**, *96*, 381–392. Sundberg, R. J.; Gupta, G. *Bioinorg. Chem.* **1973**, *3*, 39–49.
(16) Gutterman, D. F.; Gray, H. B. *Inorg. Chem.* **1972**, *11*, 1727–1733.
(17) Kincaid, J.; Stein, P.; Spiro, T. G. *Proc. Natl. Acad. Sci. U.S.A.* **1979**, *76*, 549–552.

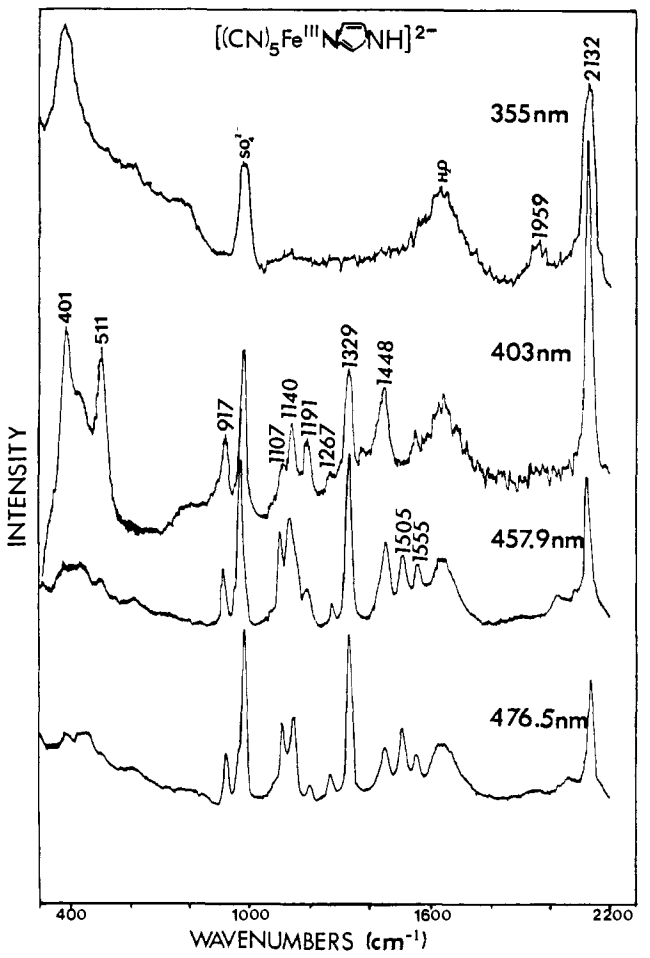

Figure 2. Resonance Raman spectra of 0.025 M $(CN)_5Fe(imH)^{2-}$ excited at 355, 403, 457.9, and 476.5 nm. The band at ca. 980 cm^{-1} derives from 0.25 M SO_4^{2-} which was used as the internal standard.

quench impurity fluorescence in these samples in order to obtain the Raman spectra.

The instrument used for the Raman spectral studies has been described in detail elsewhere.[18] A Spectra Physics Ar^+ laser was used to obtain the 457.9-, 476.5-, 488-, and 514.5-nm excitation wavelengths. Longer excitation wavelengths were generated with an Argon-ion laser excited jet stream dye laser. A Quanta-Ray Nd-Yag pumped dye laser was used in combination with nonlinear harmonic generation crystals to obtain the shorter excitation wavelengths. Most solutions were measured in a jet stream as described previously.[18] A 90° scattering geometry was employed, and an ellipsoidal mirror directed the scattered light onto the slit of a modified Spex Triplemate monochromator. A PAR OMA II intensified Reticon detector was used to detect the scattered light. The measured peak intensities were normalized to the internal standard sulfate intensities, and the data were corrected for monochromator efficiency and the ν^4 dependence. No self-absorption corrections were necessary when the jet stream was used since the small absorption path length (0.1 mm) results in negligible self-absorption. Depolarization ratios of the $(CN)_5Fe^{III}imH^{2-}$ Raman spectra were measured at selected wavelengths with a Polacoat analyzer.

Results

The electronic absorption spectra of $(CN)_5Fe(imH)^{2-}$ and $(NH_3)_5Ru(imH)^{3+}$ are shown in Figure 1. The features of these spectra have been discussed in detail previously.[4,13,15] The two lowest energy transitions (~475 and 403 nm) of the $(CN)_5Fe(imH)^{2-}$ complex have been assigned as charge-transfer transitions from imH to Fe(III).[4] These assignments were based on the sensitivity of the transition energies to deprotonation of the pyrrole hydrogen and to methyl substitution at various ring positions. The transition energies are also solvent dependent, consistent with the

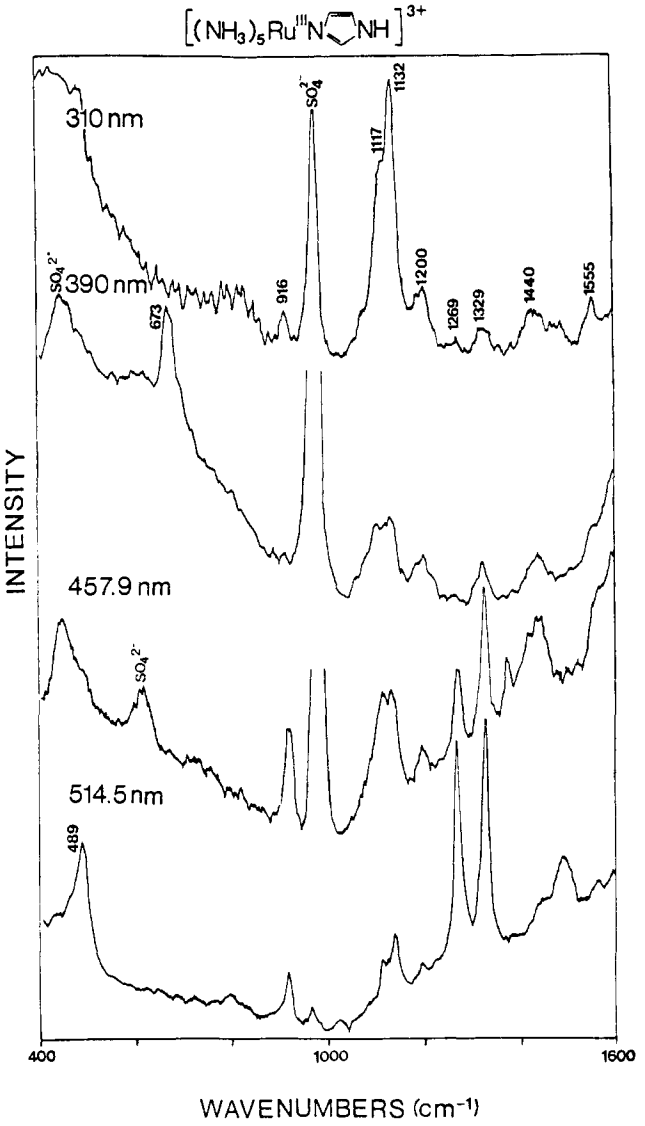

Figure 3. Resonance Raman spectra of 8.8×10^{-3} M $(NH_3)_5Ru(imH)^{3+}$ excited at 310, 390, 457.9, and 514.5 nm. The band at ca. 980 cm^{-1} derives from 0.25 M SO_4^{2-}, the internal standard. No sulfate was used in the spectrum shown for 514.5-nm excitation.

charge-transfer assignment.[19] On the basis of these observations and a comparison to work on Cu^{2+} complexes of imH,[20-22] the 475-nm band was assigned to a transition where the electron is promoted from a predominantly carbon-based imidazole orbital (π_1) while the 403-nm band was assigned to a transition from a predominately nitrogen-based imidazole orbital (π_2 and/or n).[4] The higher energy transitions observed for the Fe(III) complex are assigned to charge-transfer transitions involving the cyanide ligands. The absorption at ~350 nm in these types of complexes has been given various assignments which involve cyanide-to-iron charge transfer.[16,23] Ligand-field transitions are also expected to occur in the ~300–400 nm region.[16] Only two absorption bands are observed for $(NH_3)_5Ru(imH)^{3+}$, and these have been assigned as $d\pi_{(Ru)} \leftarrow \pi_{1(imH)}$ and $d\pi_{(Ru)} \leftarrow \pi_{2},n_{(imH)}$ for the 425- and 297-nm transitions, respectively. These assignments are analogous to the assignment of the low-energy bands in $(CN)_5Fe(imH)^{2-}$. In fact,

(18) Asher, S. A.; Johnson, C. R.; Murtaugh, J. *Rev. Sci. Instrum.* **1983**, *54*, 1657–1662.

(19) Shepherd, R. E.; Hoq, M. F.; Hoblack, N.; Johnson, C. R. *Inorg. Chem.* **1984**, *23*, 3249–3252.

(20) Fawcett, T. G.; Bernarducci, E. E.; Krogh-Jespersen, K.; Schugar, H. J. *J. Am. Chem. Soc.* **1980**, *102*, 2598–2604.

(21) Bernarducci, E.; Schwindinger, W. F.; Hughey, J. L.; Krogh-Jesperson, K.; Schugar, H. J. *J. Am. Chem. Soc.* **1981**, *103*, 1686–1691.

(22) Bernarducci, E.; Bhardwaj, P. K.; Krogh-Jespersen, K.; Potenza, J. A.; Schugar, H. J. *J. Am. Chem. Soc.* **1983**, *105*, 3866–3875.

(23) Gale, R.; McCaffery, A. J. *J. Chem. Soc., Dalton Trans.* **1973**, 1344–1351.

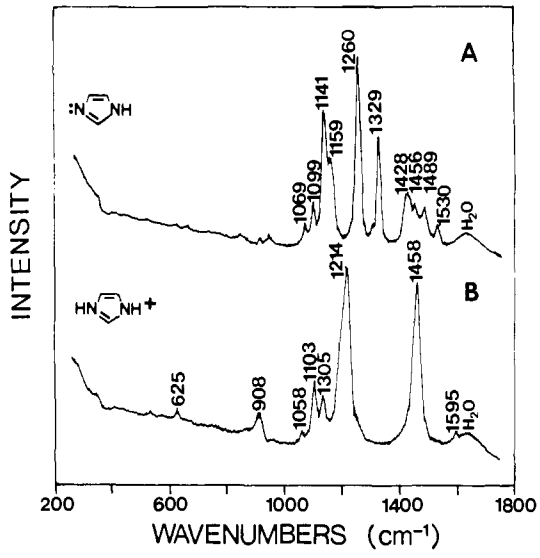

Figure 4. Raman spectra of 1 M imidazole in (A) 1.0 M NaOH and (B) 1.0 M HCl excited at 488 nm.

a strong linear correlation between the energies of the long-wavelength absorption bands of $(CN)_5FeL^{2-}$ and $(NH_3)_5RuL^{3+}$ has been demonstrated for a wide range of substituted imidazoles.[4,13]

Representative resonance Raman spectra of $(CN)_5Fe(imH)^{2-}$ and $(NH_3)_5Ru(imH)^{3+}$ with excitation within the LMCT transitions are shown in Figures 2 and 3. For comparison, normal Raman spectra of imidazole and imidazolium ion are shown in Figure 4. The peaks between 800 and 1600 cm^{-1} are due to enhanced ring stretches of the complexed imidazoles as is evident by the lack of these features in the spectra of the SCN^- and N_3^- complexes of $[(CN)_5Fe^{III}]^{2-}$ (vide infra). The intensities and frequencies of the imidazole peaks of both complexes more closely resemble the spectrum of free imidazole than that of imidazolium. Most of the bands of imidazole shift to slightly higher frequencies upon coordination. The relative intensities of the vibrational bands are different for imidazole, $(CN)_5Fe(imH)^{2-}$, and $(NH_3)_5Ru(imH)^{3+}$. The ca. 1260-cm^{-1} mode is the most intense for free imidazole (Figure 4) but is much weaker in the complexes. For $(CN)_5Fe(imH)^{2-}$ and $(NH_3)_5Ru(imH)^{2-}$ the relative intensities of the ring modes change with excitation wavelength.

Free imidazole cannot be detected at the same concentration and experimental conditions as for the complexes, indicating that the Raman intensities derive from resonance enhancement from the LMCT bands. The imidazole ring vibrations are enhanced only with excitation within the 403- and 475-nm absorption bands of $(CN)_5Fe(imH)^{2-}$. Excitation at 280 nm shows no detectable imidazole ring vibrations. With 594-nm excitation the 920-, 1267-, and 1329-cm^{-1} ring modes are observed, but with much reduced intensities. Our observation of enhancement of imidazole ring modes with excitation in resonance with the 403-nm absorption band of $(CN)_5Fe(imH)^{2-}$ directly conflicts with Walters and Spiro, who report no enhancement of imH modes with 406.7-nm excitation.[12] In contrast, our data obtained with excitation between 450 and 550 nm are similar to those of Walters and Spiro.[12]

The Raman spectra of $(CN)_5Fe(imH)^{2-}$ also show a C≡N stretching vibration at 2132 cm^{-1} and Fe—C stretching and Fe—(C≡N) bending modes at ca. 400 and 510 cm^{-1}.[24,25] The C≡N stretch is observed with all the excitation wavelengths used. In contrast, the low-frequency Fe—(C≡N) stretching and bending vibrations are only intense at excitation wavelengths shorter than ca. 450 nm. Indeed, the Fe—(C≡N) stretching and bending vibrations and the C≡N stretching vibration are the only modes observed with excitation in the 356-nm absorption band.

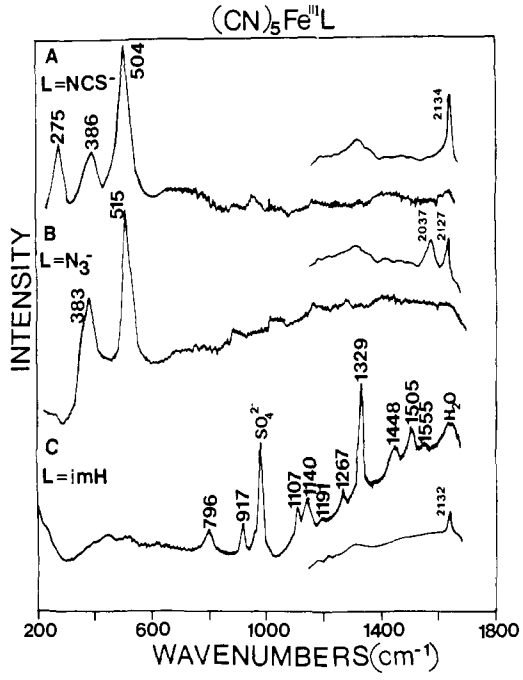

Figure 5. Resonance Raman spectra of aqueous solutions of (A) 0.02 M $(CN)_5Fe(NCS)^{3-}$, (B) 0.02 M $(CN)_5Fe(N_3)^{3-}$, and (C) 0.02 M $(CN)_5Fe(imH)^{2-}$ excited at 488 nm. The insets show the 1400–2200 cm^{-1} spectral regions.

Each of the imidazole ring vibrations and the 2132-cm^{-1} C≡N stretch were found to be polarized. The depolarization ratio of the C≡N stretching vibration shows a dependence on excitation wavelength and increases from $\rho_l = 0.17$ at 514.5 nm to 0.41 at 395 nm. The depolarization ratios for the 1267-, 1330-, 1445-, and 1505-cm^{-1} ring modes are equal to 0.33 within experimental error (±10%) for excitation at 514.5 and 403 nm. A depolarization ratio of 0.33 is the expected value when only one of the diagonal elements of the polarizability tensor differs from zero; this could occur, for example, for an electronic transition strongly polarized along the C_4 axis of the molecule (NC-Fe-imH).

We examined the resonance Raman spectra of the $(CN)_5Fe(N_3)^{3-}$ and $(CN)_5Fe(NCS)^{3-}$ complexes by exciting at 488 nm. This excitation occurs on the blue side of the LMCT transitions which involve the N_3^- and NCS^- ligands.[16] These broad LMCT bands dominate the near UV-visible absorption spectra. Figure 5 compares the 488 nm excited Raman spectra of the N_3^-, NCS^-, and imH complexes of $[(CN)_5Fe^{III}]^{2-}$. The ca. 2130-cm^{-1} C≡N stretch is enhanced for all of these complexes with 488-nm excitation; however, the Fe—(C≡N) stretching and bending vibrations at ca. 380 and 510 cm^{-1} are only enhanced for the N_3^- and NCS^- complexes. These vibrations in the imH complex show enhancement only with excitation at shorter wavelength. The NCS^- complex shows enhancement of the Fe-(NCS) stretch at 275 cm^{-1}, while the N_3^- complex shows enhancement of an asymmetric azide ligand stretching mode[16,26] at 2037 cm^{-1}. The C≡N stretch of SCN^- is not observed, presumably, because it overlaps the coordinated cyanide stretching peak.[16] An Fe–azide stretch may be buried under the Fe—C≡N band at ca. 380 cm^{-1}.[27] The other bending and stretching modes (e.g., NCS bending) present in these complexes[26] are not observed for $(CN)_5Fe^{III}N_3^-$ and $(CN)_5Fe^{III}NCS^{3-}$ with 488-nm excitation. Only particular ligand modes are resonance enhanced.

In contrast to the imH complex where numerous LMCT absorption bands overlap, the visible wavelength LMCT transitions of the N_3^- and NCS^- complexes appear to be well resolved. Thus, the enhancement of the C≡N and Fe—(C≡N) vibrations must

(24) Nakagawa, I.; Shimanouchi, T. *Spectrochim. Acta* **1970**, *26A*, 131–141.

(25) Jones, L. M. *Inorg. Chem.* **1963**, *2*, 777–780. Griffith, W. P.; Turner, G. T. *J. Chem. Soc. A* **1970**, 858–862.

(26) Nakamoto, K. "Infrared and Raman Spectra of Inorganic and Coordination Compounds"; John Wiley & Sons: New York, 1978.

(27) Gutterman and Gray (ref 16) assigned an IR band at 338 cm^{-1} to the metal–azide stretch of $[(Bu)_4N]_3[(CN)_5Fe^{III}N_3)]$. The band position may be slightly different for the complex in solution. Also see ref 26, p 278.

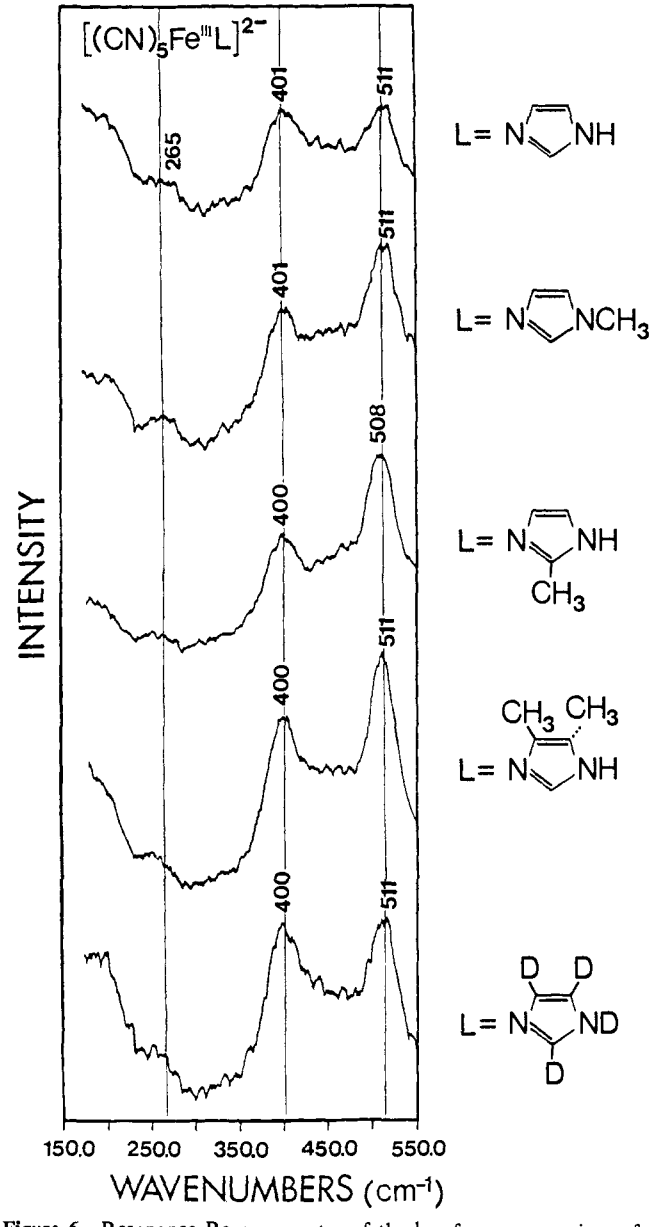

Figure 6. Resonance Raman spectra of the low-frequency regions of various imidazole derivatives of $[(CN)_5Fe^{III}]^{2-}$ (0.025 M). Excitation wavelength = 403 nm.

be due to a direct enhancement by the LMCT transitions *from* the N_3^-, NCS^-, and imH ligands and not because of the overlap of a LMCT transition *from* the CN to the iron.

As seen from Figure 5, the low-frequency modes of the imidazole complex are not significantly enhanced with 488-nm excitation, in contrast to the N_3^- and SCN^- complexes. Because of the interest in correlating the frequency of the iron–imidazole stretch to the bonding geometry of the imidazole, we carefully examined the Raman spectra in the low-frequency region of several imidazole derivatives of $(CN)_5Fe^{2-}$ with excitation within the 403 nm absorption band; the low-frequency modes are most enhanced with excitation in this band. The low-frequency Raman spectra of different methylated imidazole complexes and the deuterated imidazole complex are shown in Figure 6.

The Fe—(C≡N) stretching and bending vibrations at ca. 400 and 510 cm^{-1} are not affected by substitution on the imidazole ring. A weak vibration at ca. 265 cm^{-1} shows systematic shifts between the complexes of different imidazoles. The Rayleigh scattering background (which varies between spectra) and low intensity of the band make a precise determination of the vibrational frequency difficult; however, as indicated in Figure 6, the peak position shifts to lower frequency upon methylation of the imidazole at the 2 or 4(5) position. Deuterium substitution also causes a significant shift to lower frequency. On the basis of a simple diatomic oscillator model, we expect a shift of ca. 3.5 cm^{-1} upon deuteration if this band derives from a pure Fe–N(imidazole) stretch. For deuterium substitution any frequency shift must derive from the change in mass. The shifts occurring with methyl substitution may result from a steric effect between the methyl groups and the four planar cis cyanides and/or a change in mass. On the basis of the frequency dependence of this peak, the ca. 265 cm^{-1} band is tentatively identified as the Fe–N(imidazole) stretch.

The imidazole ring vibrations are enhanced for $(NH_3)_5Ru(imH)^{3+}$ with excitation in either the 297 or 425 nm absorption band (Figure 2). The 1117- and 1132-cm^{-1} bands are dramatically enhanced with excitation in the 297-nm LMCT band. Bands attributable to $Ru-(NH_3)$ modes are observed at 489 and 673 cm^{-1}. To verify that the enhancement observed when exciting within the 297-nm band derives from this charge-transfer absorption and not from preresonance enhancement from an imidazole $\pi^* \leftarrow \pi$ transition (further into the UV), we obtained UV resonance Raman spectra of free imidazole at several excitation wavelengths. The extent of enhancement and the relative intensity pattern of the ring modes for free imidazole with UV excitation[28] cannot account for the Raman spectra observed for the complex. The 1260-cm^{-1} mode of free imidazole is the most intense band with excitation through the UV in contrast to $(NH_3)_5Ru(imH)^{3+}$ for which it is the weakest. Thus, the UV enhancement observed for $(NH_3)_5Ru(imH)^{3+}$ must come from the charge-transfer bands.

The frequencies of Raman bands of the imidazole derivatives of $[(CN)_5Fe^{III}]^{2-}$ and $[(NH_3)_5Ru^{III}]^{3+}$ are listed in Table I. Also listed are the Raman bands of free imidazole and the imidazolate complexes, $(CN)_5Fe(im)^{3-}$ and $(NH_3)_5Ru(im)^{2+}$. Deprotonation of the pyrrole hydrogen of the imidazole results in additional frequency shifts and changes in the relative intensities of the Raman bands. Methylation of the ring dramatically effects the frequencies of the ring vibrations. These changes result from symmetry and electron-density changes in the ring which cause changes in the normal mode composition. Normal Raman data for $(CN)_5Co(imH)^{2-}$ are also included in Table I. This complex is low-spin d^6 and exhibits no low-energy LMCT transitions since no low-lying π-acceptor orbital is available.

Discussion

The Raman bands of imidazole show only small frequency shifts upon coordination to $(CN)_5Fe^{2-}$, $(NH_3)_5Ru^{3+}$, and $(CN)_5Co^{2-}$ which are similar to the shifts observed[29,30] for imidazole coordinated to Co^{2+} and Cu^{2+}. The frequencies of the ring modes are more sensitive to protonation than to coordination. Indeed, deprotonation of the coordinated imidazole also results in significant frequency shifts in the Raman bands. The small frequency shifts for the imidazole ring modes of the complex compared to free imidazole in solution indicate that little change occurs in the imidazole ground-state electronic distribution and that complexation only weakly perturbs the ring symmetry.

Excitation profiles of $(CN)_5Fe(imH)^{2-}$ and $(NH_3)_5Ru(imH)^{3+}$ are shown in Figures 7 and 8, respectively. The excitation profiles of nine imidazole ring modes and the C≡N stretch of $(CN)_5Fe(imH)^{2-}$ were measured. The corresponding ring modes were studied for $(NH_3)_5Ru(imH)^{3+}$ except for the 1505-cm^{-1} mode which was too weakly enhanced. The prominent bands of both complexes occur near 916, 1110, 1135, 1195, 1268, 1329, 1445, and 1555 cm^{-1}.

Resonance Raman enhancement occurs for those vibrations active in the resonant electronic transition. For totally symmetric modes, the enhancement depends on the oscillator strength of the electronic transition and on the Franck–Condon overlaps of the vibrational wave functions.[31] The charge-transfer transitions of

(28) Murtaugh, J. M.; Johnson, C. R.; Asher, S. A., in preparation.
(29) (a) Salama, S.; Spiro, T. G. *J. Am. Chem. Soc.* **1978**, *100*, 1105–1111. (b) Yoshida, C. M.; Freedman, T. B.; Loehr, T. M. *J. Am. Chem. Soc.* **1975**, *97*, 1028–1032.
(30) Larrabee, J. A.; Spiro, T. G. *J. Am. Chem. Soc.* **1980**, *102*, 4217–4223.

Table I

	frequencies (cm^{-1})																
A. imidazole																	
1. imH	915	1069	1099	1141	1159	1260	1329	1428	1456	1489	1530						
B. various metal centers																	
1. $(CN)_5Fe(imH)^{2-}$	917	957		1107	1140		1267	1329		1505	1555						
2. $(NH_3)_5Ru(imH)^{3+}$	916	964	1019	1117	1132	1195	1269	1329	1440	1486	1555						
3. $(CN)_5Co(imH)^{2-}$ [a]	b	952	1019	1105	1153	1183	1270	1336	1454	*b*	1550						
C. deprotonated species																	
1. $(CN)_5Fe(im)^{3-}$	919	969	1022	1104	1144	1232	1271	1309	1327	1459	1490						
2. $(NH_3)_5Ru(im)^{2+}$	917	981		1107	1141	1230	1271	1313		1459	1490						
D. deuterated derivatives[c]																	
1. $imD_{(4)}$	924		1114					1374	1427		1484	1521					
2. $imD_{(5)}^{+}$	922	953	1109	1149	1263	1288	1342		1422	1464							
3. $(CN)_5Fe(imD_{(4)})^{2-}$	920			1131	1274	1294	1352			1451							
E. methylated derivatives[d]																	
1. $(CN)_5Fe(1\text{-Me-imH})^{2-}$		959		1026	1111			1244	1287	1340	1381		1425	1477	1524	1550	
2. $(NH_3)_5Ru(1\text{-Me-imH})^{3+}$				1027	1101	1123		1251	1290	1336	1380		1420	1486		1555	1591
3. $(CN)_5Fe(2\text{-Me-imH})^{2-}$	929		985	1021		1123	1156		1298	1331		1405			1505		1578
4. $(NH_3)_5Ru(2\text{-Me-imH})^{3+}$	928			1026		1124	1154		1310			1402			1507		1584

[a] $(CN)_5Co(imH)^{2-}$ was prepared previously[4] and precipitated with dimethyldabconium ion (*N,N'*-dimethyl-1,4-diazobicyclo[2.2.2]octonium ion). [b] Raman bands of the complex were obscured by Raman bands due to dimethyldabconium ion. [c] Raman bands indicated are for the perdeuterated imidazole species. $imD_{(5)}^{+}$ is in DCl. [d] Me = methyl.

these metal complexes result in the movement of electron density from the ligand (imidazole or CN^-) to the metal center. The changes in the electron-density distribution which occur with the electronic transition result in geometric changes in the molecule between the ground and excited states. We assume that if a charge-transfer transition of an electron occurs from a particular imidazole molecular orbital to the iron the change in the electron density in bonds between imidazole atoms will be proportional to the electron density originally in the HOMO orbital involved in the transition. Those molecular vibrations which distort the ground-state geometry toward the excited-state geometry will be the most enhanced. With resonance excitation the vibrational modes enhanced involve atomic displacements of atoms involved in bonds which change in electron density. We expect imidazole vibrations to be enhanced by Fe ← imH LMCT transitions and cyanide vibrations to be enhanced by Fe ← CN LMCT transitions. The enhancement of imidazole ring modes with excitation within the two lowest energy electronic transitions of both $(CN)_5Fe(imH)^{2-}$ and $(NH_3)_5Ru(imH)^{3+}$ confirms the assignment of these bands as imidazole-to-metal charge-transfer transitions.

Examination of the excitation profiles in Figures 7 and 8, however, indicates at least two different enhancement patterns for the imidazole ring modes. Some modes, 1329 cm^{-1} for example, appear to be about equally enhanced within both imidazole charge-transfer bands. We will refer to this enhancement pattern as Class I behavior. Other modes (Class II behavior) appear to follow the absorption bands more closely and have more intensity in the higher molar absorptivity, shorter wavelength LMCT band (403 nm Fe, 297 nm Ru). Each of the imidazole ring modes is classified as to its apparent excitation profile behavior in Table II. As seen in the table and Figures 7 and 8, there is a close correlation between the excitation profiles of $(CN)_5Fe(imH)^{2-}$ and $(NH_3)_5Ru(imH)^{3+}$ for all but the 1445- and 1555-cm^{-1} modes. The 1440-cm^{-1} mode of $(NH_3)_5Ru(imH)^{3+}$ is not easily classified into either category by visual inspection. The 1555-cm^{-1} modes seem to exhibit a different behavior for the two complexes.

The two types of excitation profile behavior for the imidazole modes can be better understood by a close examination of the nature of the two LMCT transitions and of the normal modes of imidazole. The molecular orbitals of the two highest energy π-bonding orbitals of imidazole are shown in Figure 9. The molecular orbital coefficients are from Del Bene and Jaffe.[32] The π_1 orbital has more electron density from the carbon atoms and the π_2 orbital has more electron density from the nitrogen atoms. The lowest energy LMCT transition ($d\pi \leftarrow \pi_1$, 475 nm Fe, 425 nm Ru) will result in a partial depletion of bonding electron density between C_4–C_5, N_1–C_2, and N_3–C_2 in the excited state. The higher energy LMCT transition ($d\pi \leftarrow \pi_2$, 403 nm Fe, 297 nm Ru) will

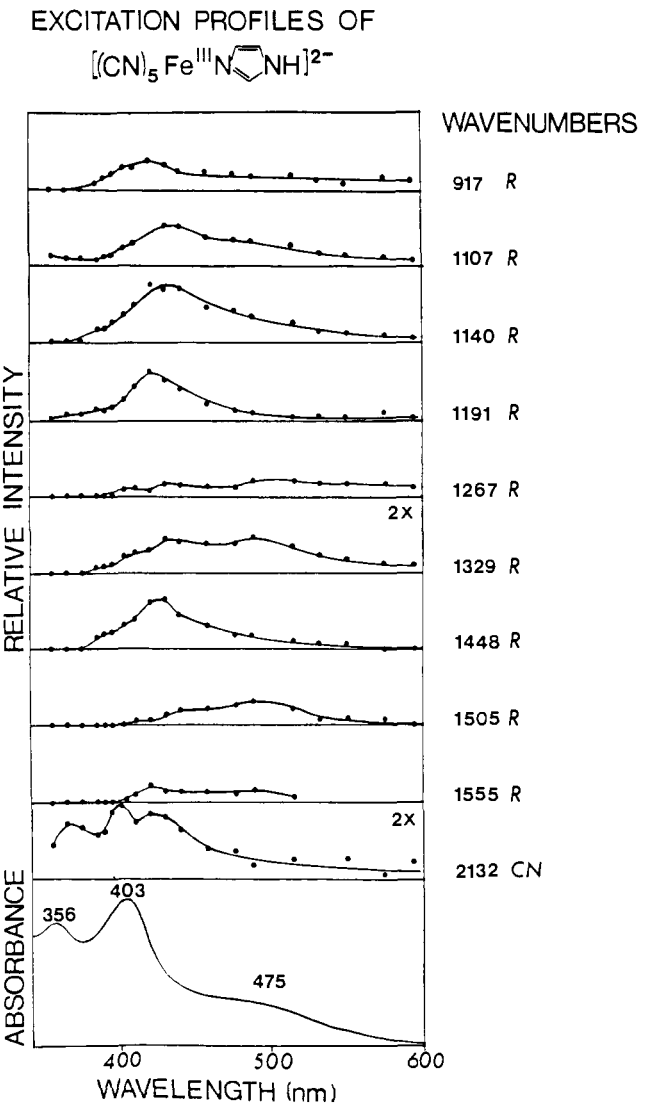

Figure 7. Raman excitation profiles of the imidazole ring modes (R) and cyanide symmetric stretching mode (CN) of $(CN)_5Fe(imH)^{2-}$. A UV–visible absorption spectrum is shown in the bottom portion of the figure for comparison. The ordinates of the profiles of the 1329- and 2132-cm^{-1} modes are twice that of the other modes.

(31) Spiro, T. G.; Stein, P. *Annu. Rev. Phys. Chem.* **1977**, *28*, 501–521.
(32) Del Bene, J.; Jaffe, H. H. *J. Chem. Phys.* **1968**, *48*, 4050–4055.

Table II

imH Raman bands (cm^{-1})	L_5M(imH) Raman bands (cm^{-1})[a]	assignment[b]	PED for stretching vibrations[c]			$(CN)_5Fe^{2-}$ class	$(CN)_5Fe^{2-}$ P	$(NH_3)_5Ru^{3+}$ class	$(NH_3)_5Ru^{3+}$ P
915	916	ω(R)	14% $\nu(N_3-C_2)$	13% $\nu(N_1-C_5, N_3-C_4)$		II	2.0	II	6.0
1099	1110	δ(R) + δ(C-H)	7% $\nu(N_3-C_2)$	25% $\nu(N_1-C_5, N_3-C_4)$		II	1.7	II	5.6
1141	1135	δ(R) + δ(C-H)	12% $\nu(N_3-C_2)$	9% $\nu(N_1-C_5, N_3-C_4)$		II	2.4	II	7.6
1159	1195	δ(R) + δ(N-H)	6% $\nu(N_3-C_2)$			II	10.0	II	6.8
1260	1268	δ(R) + $\delta(C_2-H)$	12% $\nu(N_3-C_2)$	4% $\nu(N_1-C_5, N_3-C_4)$	4% $\nu(N_1-C_2)$, 9% $\nu(C_4-C_5)$	I	1.0	I	0.71
1329	1329	δ(R) (ring breathing)		24% $\nu(N_1-C_5, N_3-C_4)$	33% $\nu(N_1-C_2)$	I	1.0	I	0.75
1428	1445	$\delta(N_1-H)$	16% $\nu(N_3-C_2)$		23% $\nu(C_4-C_5)$	II	3.5	?	2.2
1489	1505	δ(R) + $\delta(C_2-H)$		30% $\nu(N_1-C_5, N_3-C_4)$	18% $\nu(N_1-C_2)$	I	0.6		
1530	1555	δ(R) + $\delta(N_1-H)$	24% $\nu(N_3-C_2)$	19.5% $\nu(N_1-C_5, N_3-C_4)$	8% $\nu(C_4-C_5)$	I	1.5	II	4.2
expected enhancement			$d\pi \leftarrow \pi_1$ $d\pi \leftarrow \pi_2$	$d\pi \leftarrow \pi_2$	$d\pi \leftarrow \pi_1$				

[a] Approximate wavenumber positions for the Raman bands appearing in the spectra of $(CN)_5Fe(imH)^{2-}$ and $(NH_3)_5Ru(imH)^{3+}$. [b] ω = out-of-plane deformation; δ = in-plane deformation; ν = stretching. [c] Potential energy distribution from ref 33.

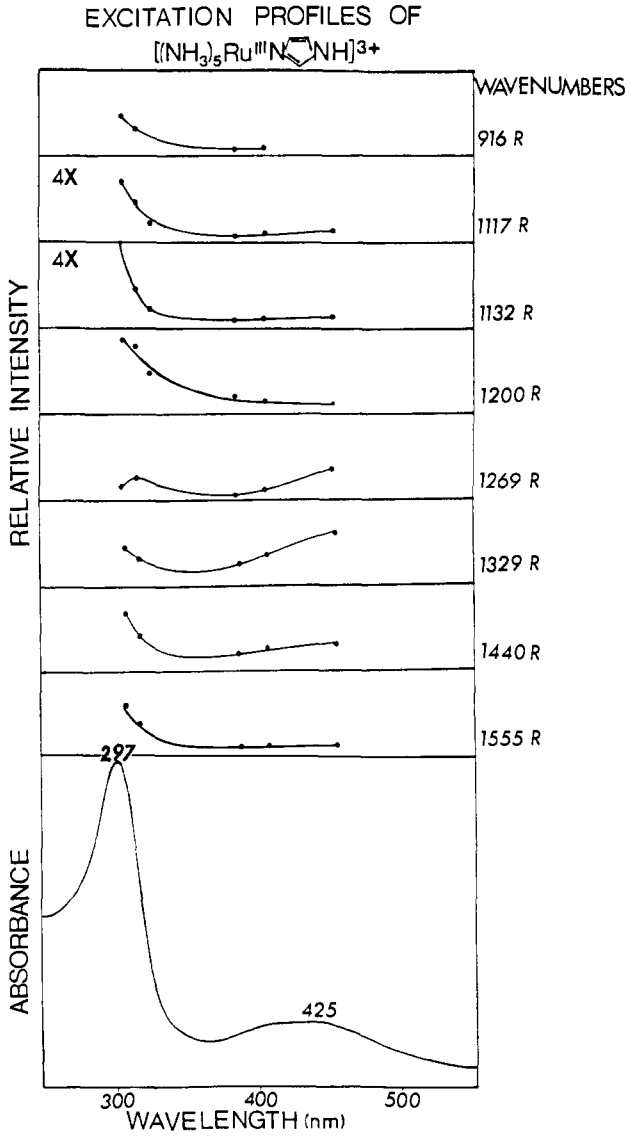

Figure 8. Raman excitation profiles of the imidazole ring modes (R) of $(NH_3)_5Ru(imH)^{3+}$. A UV-visible absorption spectrum is shown in the bottom portion of the figure for comparison. The ordinates of the profiles of the 1117- and 1132-cm^{-1} modes are four times that of the remaining modes.

result in a partial depletion of bonding electron density between N_3-C_4, N_1-C_5, and N_3-C_2. Both transitions push charge into the $d\pi$ orbitals of the metal which are nearly nonbonding to the imidazole. On the basis of the arguments presented above, the

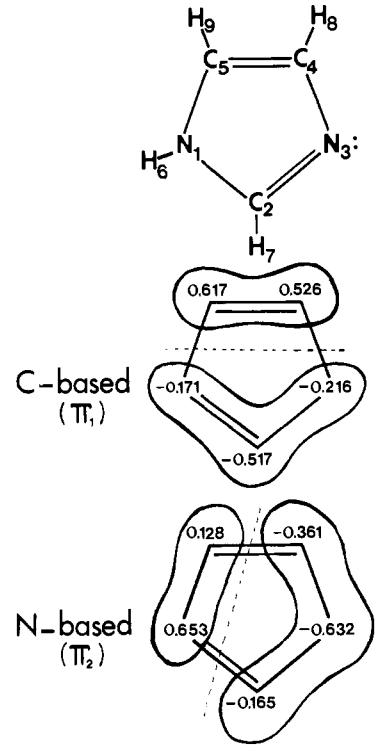

Figure 9. Molecular orbital coefficients of the π_1 and π_2 molecular orbitals of imidazole as determined by Del Bene and Jaffe.[32] Dotted lines depict nodal planes.

most enhanced modes within each transition should reflect the particular electron-density changes associated with that electronic absorption. On this basis, modes involving $\nu_{(C_4-C_5)}$, $\nu_{(N_1-C_2)}$, or $\nu_{(N_3-C_2)}$ should be most enhanced in the low energy LMCT transition and modes involving $\nu_{(N_1-C_5)}$, $\nu_{(N_3-C_4)}$, or $\nu_{(N_3-C_2)}$ should be most enhanced in the higher energy LMCT transition.

Normal mode assignments and the stretching mode contributions to the potential-energy distribution (PED) of each mode are given in Table II. The assignments are derived from the normal mode analysis of Colombo et al.[33] as modified by the deuteration study of Spiro et al.[29a] The PED's are from Colombo et al.[33] As expected for a small ring molecule like imidazole, the normal modes contain contributions from the movements of all of the atoms. Each of the modes has a large contribution from in-plane bending modes (see ref 33) in addition to the stretching modes shown in Table II. Predictions of enhancement patterns from bending mode contributions are difficult based on any simple

(33) Colombo, L.; Bleckmann, P.; Schrader, B.; Schneider, R.; Plesser, Th. *J. Chem. Phys.* **1974**, *61*, 3270-3278.

molecular orbital picture; as a result, we limit our discussion to the stretching vibrations.

The C_2–N_3 stretch contributes to all but two of the normal modes of imidazole. Because this stretch is active in both $d\pi_{(Fe)} \leftarrow \pi_{(ImH)}$ LMCT transitions it is unlikely that it will assist in the differentiation between the two classes of excitation profile behavior. The four lower frequency modes do not contain contributions from $\nu_{(C_4-C_5)}$ or $\nu_{(N_1-C_2)}$, the stretching vibrations expected to be most active in the $d\pi \leftarrow \pi_1$ transition. In contrast, the 916-, 1110-, and 1135-cm^{-1} modes contain contributions from $\nu_{(N_1-C_5)}$ and $\nu_{(N_3-C_4)}$ stretches which are active in the $d\pi \leftarrow \pi_2$ transition. These vibrations show Class II behavior.

The 1268- and 1329-cm^{-1} modes have contributions from stretching vibrations active in both the $d\pi \leftarrow \pi_1$ transition and the $d\pi \leftarrow \pi_2$ transition. Both of these modes exhibit Class I behavior. The 1268- and 1329-cm^{-1} vibrations are dominated by ring stretching and deformation and by C–H deformation. From the lack of sensitivity of these vibrations to N_1 deuteration,[29a] it is clear that displacements or distortions of the NH group are relatively unimportant. The 1195-cm^{-1} mode has no contribution from any type of stretching vibration which may distinguish its classification, but this mode clearly shows Class II behavior in both complexes. This vibration does, however, contain a significant contribution from an NH deformation and may be expected to be enhanced in the $d\pi \leftarrow \pi_2$ transition which involves the orbital with more electron density on the nitrogens. Since the 1445-, 1505-, and 1555-cm^{-1} modes have contributions from $\nu_{(C_4-C_5)}$ and $\nu_{(N_1-C_2)}$ they would be expected to exhibit Class I behavior similar to the 1268- and 1329-cm^{-1} modes. The 1445-cm^{-1} mode of $(CN)_5Fe(imH)^{2-}$ and the 1555-cm^{-1} mode of $(NH_3)_5Ru(imH)^{2-}$ do not follow the expected pattern.

Another approach to examining the different excitation profile patterns may be taken. This involves defining a parameter P which is the ratio of the maximum Raman intensity observed in the short-wavelength LMCT to the maximum intensity observed in the long-wavelength LMCT. The P values for each Raman band and each complex are given in Table II. The P values may be compared to the ratio of the oscillator strengths (f) of the two LMCT transitions as determined from a rough estimate of the area under each band. For $(CN)_5Fe(imH)^{2-}$ $f_{403}/f_{475} \approx 1.5$ and for $(NH_3)_5Ru(imH)^{3+}$ $f_{297}/f_{425} \approx 4.2$. As seen in the table, some of the P values are larger and some smaller than the corresponding ratio of oscillator strengths. Neglecting absorption spectral bandwidth differences, the Raman intensity is expected to increase with increasing oscillator strength (possibly as the square). The range of P values above suggests selectivity of the enhancement. The oscillator strength ratios provide a good differentiation between the two types of excitation profile behavior. In general, Class II profiles have P values greater than the ratio of oscillator strengths, suggesting some selective relative enhancement in the $d\pi \leftarrow \pi_2$ transition and Class I profiles have P values less than the ratio of oscillator strengths, suggesting selective relative enhancement in the $d\pi \leftarrow \pi_1$ transition.

The agreement between predictions based on the normal mode analysis and the observed excitation profile behavior is reasonable and relatively self consistent. Only the 1445- and 1555-cm^{-1} modes seem to deviate from expectations. Several points regarding these modes should be made. On the basis of deuteration studies, Spiro et al. have found that the 1535-cm^{-1} (1555 cm^{-1} for the coordinated imidazoles) mode of imidazole is sensitive to N_1 deuteration.[29a] This is inconsistent with the PED's calculated by Colombo et al.[33] These deuteration studies prompted Spiro et al. to make minor changes in the assignments of some imidazole modes.[29a] Secondly, the modes which show the largest frequency shifts upon coordination are the imidazole 1160-, 1430-, 1490-, and 1535-cm^{-1} modes. These same modes also show the largest variability in frequency between different metals (see Table I and ref 29 and 30). This suggests the possibility of some change in normal mode composition. Our discussion is based on the assumption that the normal mode calculation for free imidazole can be directly applied to the complexes and that a molecular orbital calculation of free imidazole is directly applicable to coordinated imidazole. These assumptions are reasonable because relatively small shifts of the imidazole frequencies occur upon coordination and because imidazole is not a strong π-bonding ligand. In view of these approximations the consistencies between prediction and observation confirm the assignment of the long-wavelength LMCT as the $d\pi_{(Fe)} \leftarrow \pi_{1(ImH)}$ transition and the shorter wavelength LMCT as $d\pi_{(Fe)} \leftarrow \pi_{2(ImH)}$ transition.

As seen in Figure 7, the C≡N stretch of $(CN)_5Fe(imH)^{2-}$ is also enhanced with excitation within the imidazole LMCT bands. Cyanide is known to be a very strong π-bonding ligand.[34] The LMCT transition places additional electron density in the $d\pi$ orbitals in the excited state. This orbital is delocalized over the cyanides, and it is reasonable that resonance enhancement of cyanide modes would occur. There is also enhancement of $\nu_{(C\equiv N)}$ within the 356-nm band where no imidazole ring mode enhancement occurs. This confirms the assignment of this band as $d\pi_{(Fe)} \leftarrow CN^-$. Gutterman and Gray's[16] study of the SCN^- and N_3^- complexes suggests a $d\pi_{(Fe)} \leftarrow \sigma_{CN^-}$ transition should occur at this wavelength. The $\nu_{(C\equiv N)}$ excitation profile appears to show two maxima within the 403-nm band. This may be due to a ligand-field transition in this region,[16,35] but we do not feel that the quality of our data is sufficient to confirm this. The enhancement of the low-frequency iron–cyanide modes with excitation at these wavelengths may also be due to this transition. The dispersion of the depolarization ratio of $\nu_{(C\equiv N)}$ may be due to contributions from these transitions; unfortunately, the magnitude or signs of these contributions cannot be predicted.

The assignment of the iron–histidine stretching mode of deoxy myoglobin was recently confirmed.[37] The collective data from Raman studies of deoxy myoglobin, deoxy hemoglobin, and model iron(II) heme complexes indicate that a band in the 210–230 cm^{-1} region is due to the Fe–N(histidine) stretch.[37] Our tentative assignment of the weak band at ca. 265 cm^{-1} for $(CN)_5Fe(imH)^{2-}$ as the Fe–N(imH) stretch seems reasonable. A shift of ~35 cm^{-1} to higher frequency could be expected for an Fe(III) vs. an Fe(II) complex. The poor enhancement from the $d\pi_{(Fe)} \leftarrow$ imH LMCT transition will make this mode difficult to detect in biological systems. Low-frequency porphyrin modes are likely to obscure the observation of this Fe–imH stretch in Fe(III) heme proteins.

In heme proteins intense porphyrin ring modes are likely to dominate the Raman spectrum in the 700–1600 cm^{-1} region where imidazole ring modes occur. For $(CN)_5Fe(imH)^{2-}$ the imidazole ring modes are only modestly enhanced by exciting within the two Fe ← imH charge-transfer transitions. The 1330 cm^{-1} ring breathing mode, the most intense imidazole ring vibration, exhibits an intensity maximum at an excitation wavelength of 430 nm. The absolute Raman cross section of the 1330-cm^{-1} mode can be calculated, using the recently determined values of the absolute cross section of sulfate.[36] The absolute Raman cross section of this mode is 3.4×10^{-28} cm^2/molecule·steradian at 430 nm. Bangcharoenpaurpong et al. recently reported a Raman cross section for the 1357-cm^{-1} porphyrin ring breathing mode of deoxy myoglobin of ca. 3×10^{-24} cm^2/molecule·steradian with 430-nm excitation.[9] It is clear that the maximum enhancement of imidazole ring modes in the $d_{\pi(Fe)} \leftarrow$ imH LMCT transitions is much less (ca. 10^4) than the enhancement of the heme modes by the heme Soret band. However, it is possible that Fe(heme) ← imH(histidine) LMCT transitions in heme proteins could occur with higher molar absorptivities than those in $(CN)_5Fe(imH)^{2-}$ and result in much larger Raman enhancements of imH ring modes.

Conclusions

Excitation within the two LMCT bands of $(CN)_5Fe(imH)^{2-}$ and $(NH_3)_2Ru(imH)^{3+}$ results in only modest enhancement of the imidazole ring modes as observed earlier for $(CN)_5Fe(imH)^{2-}$

(34) Sharpe, A. G. "The Chemistry of Cyano Complexes of the Transition Metals"; Academic Press: New York, 1976.
(35) Hrepic, N. V.; Malin, J. M. *Inorg. Chem.* **1979**, *18*, 409–413.
(36) Dudik, J. M.; Johnson, C. R.; Asher, S. A. *J. Chem. Phys.* **1985**, *82*, 1732–1740.
(37) Argade, P. V.; Sassaroli, M.; Rousseau, D. L.; Inubushi, T.; Ikeda-Saito, M.; Lapidot, A. *J. Am. Chem. Soc.* **1984**, *106*, 6593–6596.

by Walters and Spiro.[12] The LMCT absorptions for $(CN)_5Fe(imH)^{2-}$ have molar absorptivities on the order of ~1000 and ~300 for the short- and long-wavelength absorption bands, respectively. These are particularly low for charge-transfer transitions but are characteristic for the $(CN)_5Fe(imH)^{2-}$ complexes. In heme proteins the vibrational enhancement due to the heme $\pi^* \leftarrow \pi$ transitions is likely to mask the imidazole ring modes even if those modes was resonantly enhanced by an Fe-histidine charge-transfer band.

Resonance Raman data confirm the previous assignments of the 403- and 475-nm electronic absorptions as deriving from LMCT transitions involving the carbon and nitrogen-based π-imidazole orbitals to the iron. The excitation profile patterns can be used to examine which imidazole π orbitals are involved in particular LMCT transitions. The imidazole charge-transfer excited states of $(CN)_5Fe(imH)^{2-}$ involve the CN ligands as evidenced by both the excitation profile of the 2132-cm^{-1} C≡N stretch and the spectral behavior of the Fe—C stretching and Fe—(C≡N) bending modes. The data also support the assignment of the electronic absorption band at 356 nm as a LMCT transition from the CN ligands to the iron.

Enhancement of the Fe-N(imH) stretching vibration is weak. Although the frequencies of the imidazole vibrations are sensitive to protonation of the pyrrole nitrogen (and presumably the hydrogen bonding at this nitrogen), new environmental information from the imidazole vibrations in the heme proteins is, unfortunately, not likely to derive from Raman studies which excite in the LMCT transitions which involve the two HOMO's of the imidazole ring of the proximal histidine. The Raman intensities are much too weak. However, it is possible that higher energy LMCT transitions will give much larger Raman enhancements.

Acknowledgment. We thank Thanh Phung and Maryann Fundy for their technical assistance. We gratefully acknowledge partial support of this work from NIH grant IR01GM30741-03. Sanford A. Asher is an Established Investigator of the American Heart Association; this work was done during the tenure of an Established Investigatorship of the American Heart Association and with funds contributed in part by the American Heart Association, Pennsylvania affiliate.

Registry No. $(CN)_3Fe(imH)^{2-}$, 61332-60-3; $(NH_3)_5Ru(imH)^{3+}$, 80593-52-8; histidine, 71-00-1.

Isomerization of Cyclopropylidene to Allene

Arvi Rauk,*[1a] Willem J. Bouma,[1b] and Leo Radom

Contribution from the Research School of Chemistry, Australian National University, Canberra, A.C.T. 2601, Australia. *Received January 24, 1985*

Abstract: The isomerization of cyclopropylidene to allene has been investigated by ab initio methods. Analytical gradient techniques are used to locate stationary structures on the reaction potential hypersurface, and vibrational frequency analysis is used to characterize the structures as minima or saddle points as well as to provide an estimate of the zero-point corrections to the adiabatic surface. On the singlet potential energy surface, rearrangement of cyclopropylidene to allene involves a barrier of 48 kJ mol^{-1}. The transition structure is asymmetric with a CCC bond angle of 96° and asymmetrically disrotated methylene groups. The overall reaction is exoergic by 270 kJ mol^{-1}. The results are consistent with experimental observations for substituted, chiral cyclopropylidenes. The previously postulated bent-planar open-shell singlet structure is confirmed as the transition structure for internal rotation in allene. The calculated barrier for this process is 201 kJ mol^{-1}. The isomerization of tri cyclopropylidene to triplet allene is hindered by a barrier of 99 kJ mol^{-1}. The transition structure is a nonrotated structure with unequal C-C bond lengths and a plane of symmetry. The reaction on the triplet potential surface is exoergic by 105 kJ mol^{-1}.

The ring opening of cyclopropylidenes (or the corresponding carbenoids) to yield allenes was first reported by Doering[2] in 1958 and has been extensively exploited as a convenient route to the preparation of cyclic[3,4] and acyclic[5-7] optically active allenes. The retention of optical activity negates the possibility that planar (and therefore achiral) structures are involved in the conversion. The reaction proceeds with a high degree of stereospecificity in the case of anti-substituted cyclopropylidenes, and the configuration of the product allene is that expected if the reaction proceeds via a conrotatory motion under steric control.[5,6] Although a sum of 90° is required for the rotations of the two terminal groups in order that the final configuration be achieved, the two groups need not, and in an asymmetric molecule will not, rotate by the same amount. The "conrotatory" mechanism merges with a "nonrotatory" mechanism in the extreme case where only one of the two groups rotates. In syn-disubstituted cyclopropylidenes, neither direction of conrotatory motion is favored by steric factors. However, resolved syn-substituted cyclopropylidenes also yield optically active allenes. In this case, the degree of stereoselectivity

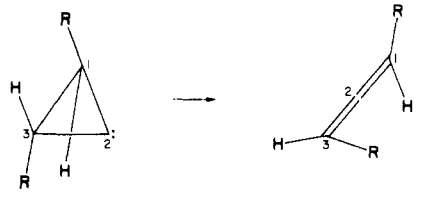

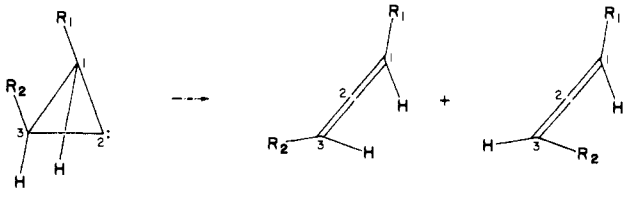

appears to be much lower.[7] Borden[8] has suggested that a monorotatory mechanism under electronic control may be operating. Other initial motions of the nuclei may also be envisaged, for example, corresponding to disrotatory or nonrotatory ring opening. These also are compatible with the results of stereochemical

(1) (a) On sabbatical leave from the Department of Chemistry, University of Calgary, Calgary, Alberta, Canada. (b) Present address: CSIRO Division of Atmospheric Research, Aspendale, Victoria, Australia.
(2) Doering, W. von E.; Laflamme, P. M. *Tetrahedron* **1958**, *2*, 75.
(3) Cope, A. C.; Moore, W. R.; Bach, R. D.; Winkler, H. J. S. *J. Am. Chem. Soc.* **1970**, *92*, 1243.
(4) Moore, W. R.; Bach, R. D. *J. Am. Chem. Soc.* **1972**, *94*, 3148.
(5) Jones, W. M.; Wilson, J. W., Jr. *Tetrahedron Lett.* **1965**, 1587.
(6) Walbrick, J. M.; Wilson, J. W., Jr.; Jones, W. M. *J. Am. Chem. Soc.* **1968**, *90*, 2895.
(7) Jones, W. M.; Krause, D. L. *J. Am. Chem. Soc.* **1971**, *93*, 551.
(8) Related in ref 7.

0002-7863/85/1507-3780$01.50/0